when the ferroelectric is poled positive (Fig. 4A) and to decrease when it is poled negative (Fig. 4B). The device clearly behaves (Fig. 3) as one would expect if the channel modulation was the result of a field effect.

We measured no change in channel resistance after shorting the top and bottom electrodes through a 1-megohm resistor. We measured only a 3% change in the channel resistance after waiting 45 min at room temperature. Capacitance verses bias voltage curves for a PZT/LCMO capacitor (PZT, lead zirconate titanate) grown under the same conditions as the FET devices (Fig. 5) show ferroelectric switching rather than charge injection. The higher capacitance at negative bias voltage, as compared to positive bias voltage, is consistent with the formation of a depletion layer in a *p*-type semiconductor. These observations indicate that the channel modulation is in fact caused by a field effect and not "charge-up" or charge injection.

The present results demonstrate that a markedly improved, nonvolatile ferroelectric field effect device can be constructed of perovskite heterostructures with a magnetoresistive manganate as the channel semiconductor. The enhanced interface characteristics associated with the ferroelectric-manganate interface allows for the fabrication of field effect devices with channel-resistance modulation of at least a factor of 3 and retention on the order of hours.

REFERENCES AND NOTES

1. R. Ramesh *et al.*, *Appl. Phys. Lett.* **64**, 1588 (1994).
2. P. M. Heyman and G. H. Heilmeier, *Proc. IEEE* **54**, 842 (1966).
3. S. Jin *et al.*, *Science* **264**, 413 (1994).
4. S. B. Ogale *et al.*, *Phys. Rev. Lett.* **77**, 1159 (1996).
5. D. H. Looney, U.S. Patent 2 791 758 (1957); W. L. Brown, U.S. Patent 2 791 759 (1957); I. M. Ross, U.S. Patent 2 791 760 (1957); J. A. Morton, U.S. Patent 2 791 761 (1957).
6. C. H. Ahn *et al.*, *Science* **269**, 373 (1995).
7. Y. Watanabe, *Appl. Phys. Lett.* **66**, 1770 (1995).
8. R. Ramesh *et al.*, *Science* **252**, 944 (1991).
9. The ferroelectric layers were patterned by in situ mechanical masking. The semiconductor channel and electrodes were patterned with photolithographic wet etch and lift-off techniques, respectively. Samples were then photolithographically patterned again and ion-milled in order to isolate individual devices. The perovskite semiconductor layer, LCMO, was between 300 to 500 Å thick. The ferroelectric layer, PZT, was between 3000 and 4000 Å in thickness. Platinum electrodes, 1000 Å in thickness, were deposited ex situ after the patterning of the other layers. Analysis by x-ray diffraction, performed before patterning and electrode deposition, indicated that no undesirable phases were formed and that both the LCMO and PZT were well-oriented with strong [001] texture. Rutherford backscattering data confirmed that the film stochiometry was consistent (within error) with that of the target materials. Transmission electron microscopy showed that the interfaces were sharp and smooth with no significant interdiffusion or formation of secondary phases. Pulsed hysteresis loops were acquired at room temperature with a Radiant Technologies RT-66A measurement system in order to determine the ferroelectric properties of the PZT layer.
10. The hysteresis loops in Figs. 1 and 3 are shifted slightly toward negative gate voltages. We attribute this shift to the fact that the top and bottom electrodes are made of different materials. Because the carrier concentration and electronic work function of the top and bottom electrodes are different, we expect this type of asymmetry in the hysteresis of the devices.
11. S.M. and R.R. would like to acknowledge the support of the U.S. Department of Army Federated Laboratories. T.V. would like to acknowledge the support of NSF grant DMR 9404579.

26 August 1996; accepted 12 February 1997

Melting Temperature and Partial Melt Chemistry of H_2O-Saturated Mantle Peridotite to 11 Gigapascals

Tatsuhiko Kawamoto and John R. Holloway*

The H_2O-saturated solidus of a model mantle composition (Kilborne Hole peridotite nodule, KLB-1) was determined to be just above 1000°C from 5 to 11 gigapascals. Given reasonable H_2O abundances in Earth's mantle, an H_2O-rich fluid could exist only in a region defined by the wet solidus and thermal stability limits of hydrous minerals, at depths between 90 and 330 kilometers. The experimental partial melts monotonously became more mafic with increasing pressure from andesitic composition at 1 gigapascal to more mafic than the starting peridotite at 10 gigapascals. Because the chemistry of the experimental partial melts is similar to that of kimberlites, it is suggested that kimberlites may be derived by low-temperature melting of an H_2O-rich mantle at depths of 150 to 300 kilometers.

H_2O lowers melting temperatures of mantle peridotites and also affects the chemistry of their partial melts (*1*, *2*). Earlier experiments demonstrated that partial melting of H_2O-saturated peridotite produces andesitic or dacitic melts at 1 GPa, in contrast to basaltic melts in dry peridotite (*2*). Therefore, it was surprising that partial melting of H_2O-saturated peridotites at pressures greater than 5 GPa produced ultramafic melts (*3*, *4*). Two ultramafic magma types are known on Earth: komatiites and kimberlites. Komatiites are believed to represent high-temperature melts in the early Earth. However, recent experiments (*3*, *4*) led to suggestions that komatiites could be produced by wet peridotite melting (*3*–*5*), and hence they could shed light on the degassing history of Earth's mantle (*6*). Kimberlites contain diamonds and peridotite nodules that are the only samples from the mantle's deepest depths (~150 to 200 km). Understanding the origin of these ultramafic magmas would provide important clues to the evolution of Earth's mantle.

In an effort to understand the effect of H_2O on the generation of ultramafic magmas, we undertook a precise determination of solidus temperatures and partial melt chemistry in an H_2O-saturated peridotite. The starting material was a mixture of an Mg-free KLB-1 peridotite gel and brucite, resulting in molar ratios of 89 for Mg/(Mg + Fe) × 100 (Mg#) and 1.46 for (Mg + Fe)/Si, with an H_2O content of 13.7% (by weight). The chemistry of KLB-1 peridotite is similar to that of pyrolite mantle (*7*). The ground starting material was put in a thick-walled Ag capsule with a few pieces of folded Ag foil (0.05 mm thick) (Fig. 1A). The foil was used to extract partial melts by capillary action (*8*). This sample assembly was placed inside a box-shaped graphite furnace. We used Ag to minimize Fe loss to the capsule and maximize thermal conductivity. The temperature was monitored by an S-type thermocouple placed at the top of the sample assembly, and the thermal gradient along the sample (0.5 mm long) was estimated to be <50°C (*9*). We heated samples to temperatures from 950° to 1100°C at pressures from 5 to 11 GPa (Table 1).

We determined the solidus temperature by observing the dendritic texture of quenched partial melts associated with the Ag foils (Fig. 1B) and the increase in the Mg# of olivine crystals with increasing temperature (Table 1). Because Fe is partitioned into the melt relative to coexisting olivine, an increase of Mg# in the olivine is an indicator of partial melting. In some experimental products, we did not observe any dendritic texture, although the Mg# of olivine had higher values than those of lower temperature runs. In those cases, we

---

T. Kawamoto, Department of Geology, Arizona State University, Tempe, AZ 85287, USA.
J. R. Holloway, Departments of Geology and Chemistry, Arizona State University, Tempe, AZ 85287, USA.

*To whom correspondence should be addressed. E-mail: john.holloway@asu.edu

Table 1. Summary of experimental conditions, mineral assemblages, and chemistry of partial melts. Ol, olivine; En, enstatite; Di, diopside; Gt, garnet; L, liquid; CH, clinohumite; PhE, phase E; Mg#, Mg/(Mg + Fe) atomic ratio × 100. Chemical compositions of partial melt are normalized to 100 total. K_D values represent distribution coefficients of FeO and MgO between residual olivine and partial melts (FeO/MgO) of olivine/(FeO*/MgO) of melt from mass-balance calculation (percent by weight). Analytical conditions were 15 kV accelerating voltage and 10 nA specimen current. Chemical compositions of crystals and dendritic portions were measured by focused beam and over a 30 μm by 40 μm scanning area, respectively. Numbers in parentheses represent ±1 SD from the mean of five or more analyses.

P (GPa)	*T* (°C)	*t* (hours)	Phases and modal compositions	Mg# of Ol	SiO_2	TiO_2	Al_2O_3	FeO*	MgO	CaO	Na_2O	Raw total	Mg#	(Mg + Fe)/Si	K_D
5	1000	20	Ol, En, Di, Gt	90.9											
5	1050	22	L (25), Ol (50), En (17), Gt (8)	91.5	42.8 (3.9)	0.55 (0.07)	5.3 (0.4)	12.5 (1.1)	25.2 (2.2)	13.2 (3.4)	0.47 (0.07)	43.0	78.2 (0.1)	1.12 (0.03)	0.333
5	1100	5	L (37.5), Ol (50), En (12), Gt (0.5)	91.3	44.1 (3.9)	0.46 (0.04)	8.6 (0.6)	11.0 (0.6)	25.5 (1.4)	9.5 (1.2)	0.90 (0.08)	52.7	80.7 (0.1)	1.07 (0.04)	0.398
7.5	1000	3	Ol, En, Di, Gt	91.1											
7.5	1050	16	L (17), Ol (51), En (15), Di (4), Gt (13)	91.6	42.2 (3.0)	0.59 (0.05)	3.3 (0.3)	13.5 (1.3)	27.0 (2.8)	12.7 (1.6)	0.86 (0.11)	53.9	78.1 (0.1)	1.22 (0.13)	0.328
7.5	1100	15.3	L (30), Ol (22), En (38), Gt (10)	92.8	37.6 (3.7)	0.53 (0.01)	3.1 (0.3)	14.0 (1.1)	32.3 (3.4)	12.0 (1.9)	0.38 (0.09)	52.7	80.4 (0.4)	1.61 (0.16)	0.319
10	1000	42	Ol, En, Di, Gt	91.3											
10	1000	20.7	Ol, En, Gt	93.0											
10	1050	20.5	L (29), Ol (28), En (30), Gt (13)	93.6	33.9 (1.6)	0.64 (0.16)	1.9 (0.1)	17.1 (1.7)	36.5 (3.7)	9.3 (4.7)	0.59 (0.12)	39.7	79.1 (0.1)	2.03 (0.11)	0.259
10	1100	16	L (37), Ol (23), En (27), Gt (13)	95.8	35.9 (5.7)	0.40 (0.11)	2.1 (0.3)	14.6 (2.7)	35.4 (5.5)	11.3 (2.4)	0.31 (0.08)	53.7	81.2 (0.3)	1.81 (0.14)	0.190
11	950	38	En, Di, Gt, CH, PhE												
11	1000	10	En, Di, Gt, CH, PhE												
11	1050	20.3	Ol, En, Gt	93.8											
11	1100	13.5	L (33), Ol (22), En (30), Gt (15)	94.6	33.4 (2.3)	0.45 (0.08)	2.3 (0.9)	14.9 (1.3)	37.8 (3.0)	10.6 (5.1)	0.50 (0.20)	50.4	81.9 (0.3)	2.07 (0.14)	0.258

interpreted those runs to be above the solidus. We determined the major oxide compositions of all phases by means of an electron microprobe (Table 1). We calculated degrees of melting for supersolidus runs with least-squares fitting, using major oxide concentrations in all the phases (Table 1). The amount of H_2O available to the melt in these experiments ranged from 34 to 80% by weight. The quenched melt phase showed a dendritic texture of crystals, which is typical for a quenched liquid at high pressures. No evidence for a solute-rich aqueous fluid was observed, so we cannot be certain that the silicate melt was saturated in H_2O, but it was certainly H_2O-rich and probably H_2O-saturated.

The solidus of H_2O-saturated KLB-1 shows no appreciable change in temperature from 5 to 11 GPa (Fig. 2). In the dry KLB-1 system the solidus temperature monotonously increases from 1730°C at 5 GPa to 1950°C at 10 GPa (*10*). Therefore, the addition of H_2O results in a drop in solidus temperature of almost 1000°C at 10 GPa. A higher solidus temperature was reported for a less refractory peridotite nodule (Mg# = 85) at 2 to 6 GPa under H_2O-saturated conditions (*1*). A higher solidus for a synthetic pyrolite mantle similar in composition to KLB-1 peridotite was also reported at 5.5 and 7.7 GPa under H_2O-saturated conditions (Fig. 2) (*3*). The difference in wet solidus temperatures between the earlier experiments and ours may be attributable to Fe loss to Pt capsules in the earlier experiments and also to a greater ability to detect melting with our capillary system. The present results are supported by the differences in subsolidus phase assemblage: Inoue and Sawamoto (*3*) reported that the subsolidus was olivine, enstatite, and garnet, whereas in our experiments the assemblage included diopside in addition to those three minerals, as expected in near-solidus experiments. At 11 GPa, our solidus temperature encounters the stability field of dense hydrous Mg-Fe silicates such as clinohumite and phase E (*11*), and the solidus temperature may increase (Fig. 2).

At 12 GPa the wet solidus should intersect the stability field of the β phase of olivine (*12*), which can contain as much as 3% H_2O by weight (*5*, *6*). Phase E is stable from 9 GPa to at least 17 GPa, and above 17 GPa phase F and superhydrous phase B coexist with phase E in the KLB-1 system. Because phase E, phase F, and superhydrous phase B can store ~7.4%, ~15%, and ~10% H_2O by weight (*4*, *5*, *13*), respectively, peridotitic mantle is unlikely to be H_2O-saturated at pressures greater than 11 GPa.

Above the solidus, H_2O is preferentially partitioned into partial melts. Therefore, if the total H_2O content of the solid mantle is not more than what can be accommodated in the hydrous minerals, the possible pressure and temperature range of free H_2O fluid is bounded by the stability fields of pargasite, chlorite, antigorite (*14*), chondrodite, clinohumite, phase E (*6*), the β phase of olivine (*12*), and the H_2O-saturated solidus of mantle peridotite (Fig. 2). This pressure-temperature region delimits a maximum field for H_2O-rich fluid in the upper mantle but does not require its presence.

The (Mg + Fe)/Si molar ratio of the partial melts of H_2O-saturated KLB-1 peridotite monotonously increases from 0.2 (andesitic composition) at 1 GPa (*15*) to 1 (pyroxene) at 5 GPa and to 2 (olivine) at 10

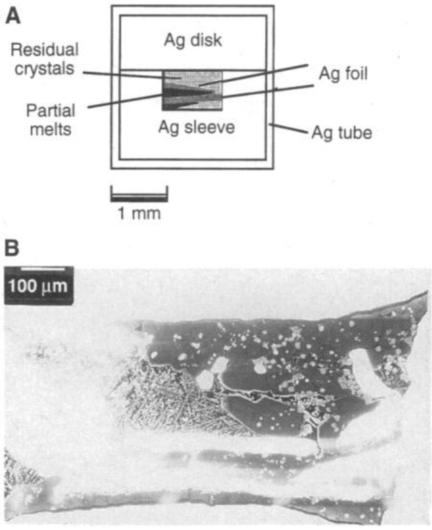

Fig. 1. (**A**) Schematic cross section of the experimental capsule. (**B**) Backscattered electron image of a sample at 1100°C and 7.5 GPa. Dendritic texture is observed associated with Ag foils (white).

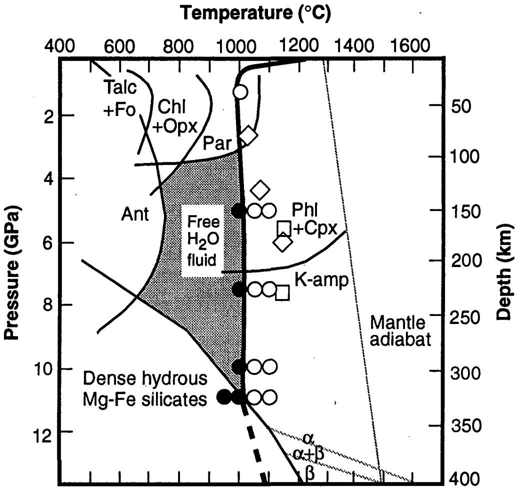

Fig. 2. Pressure-temperature projection of the solidus of H_2O-saturated KLB-1 peridotite. Open circles represent the phase assemblage of liquid, olivine, garnet, and Ca-poor pyroxenes, with or without Ca-rich pyroxene. Filled circles represent subsolidus assemblages: olivine, garnet, and two pyroxenes at 5 to 10 GPa; clinohumite, phase E, garnet, and two pyroxenes at 11 GPa. Previous solidus determinations are shown as open squares (*3*) and diamonds (*1*). The thick gray curve designates the H_2O-saturated KLB-1 solidus. The curve is solid where it is defined by our experiments and dashed at higher pressure where no precise experimental data exist. At 1 GPa the solidus temperature is below 1000°C (*15*). The possible pressure and temperature range of free H_2O fluid is bounded by the stability fields of pargasite (Par), chlorite (Chl), antigorite (Ant) (*14*), chondrodite, clinohumite, phase E (*6*), the β phase of olivine (*12*), and the H_2O-saturated solidus of mantle peridotite. Phase boundaries among α, α + β, and β phases of $(Mg_{0.9}Fe_{0.1})_2SiO_4$ are adapted from Katsura and Ito [see (*12*)]. Opx, orthopyroxene; Phl, phlogopite; Cpx, clinopyroxene; K-amp, potassium-richterite; Fo, forsterite.

GPa (Fig. 3). Because KLB-1 itself has a (Mg + Fe)/Si molar ratio of 1.46, the partial melts are more ferromagnesian than the bulk system at 10 GPa. A similar change in initial melts was also reported in the $MgO-SiO_2-H_2O$ system at (*16*). This change is surprising when compared to the much smaller change seen in dry melts: an (Mg + Fe)/Si molar ratio of 1 at 5 GPa, 1.1 at 10 GPa, and 1.1 at 18 GPa (*17*). Although the lack of spectroscopic observation of these wet melt compositions prevents any conclusive explanation of this conspicuous feature, it is likely that the structure of wet silicate melts changes drastically as a function of pressure.

The distribution coefficient of FeO versus MgO between residual olivine and partial melts (K_D) (*18*) decreases from 0.36 at 5 GPa to 0.33 at 7.5 GPa, and to 0.25 at 11 GPa (Table 1). In earlier studies, K_D was found to vary from 0.3 in quartz tholeiite basalt to 0.25 in nephelinite and to decrease with the addition of Fe_2SiO_4 olivine component to peridotitic or komatiitic systems (*18*). Thus, the decrease of K_D with increasing pressure in our experiments may be the result of decreasing polymerization (increasing olivine component) of the partial melts with increasing pressure.

The partial melts from our experiments show an increase in MgO and FeO* (total iron as FeO) and a decrease in SiO_2 and Al_2O_3 with increasing pressure (Fig. 4). The ratio of CaO to Al_2O_3 increases with increasing pressure, whereas CaO concentrations are nearly constant. Similar chemical changes as a function of pressure were observed in dry KLB-1 (*17*). However, the variations were greater in the wet system; for example, the CaO/Al_2O_3 ratio changed from 1 at 5 GPa to 4 at 7.5 GPa in the wet system, and, in contrast, from 1 at 5 GPa to 2.2 at 9.7 GPa in the dry system. Wet melts are characterized by higher MgO, CaO, and CaO/Al_2O_3 and lower SiO_2, Al_2O_3, and FeO* than dry melts at the equivalent pressures (Fig. 4) (*17*). Except for CaO, the changes resulting from the addition of H_2O are the same as those caused by increasing pressure in the dry system. Therefore, it might be difficult to distinguish the effects of pressure and H_2O.

The experimental partial melts have lower SiO_2 and higher CaO than komatiites (Fig. 4). Therefore, our study indicates that the melting of H_2O-rich (13.7% by weight) mantle is not likely to produce komatiite. H_2O-undersaturated peridotite is more likely to be a source for komatiites. This result is consistent with recent H_2O measurements of melt inclusions in olivine of komatiites [0.2 to 1.0% by weight (*19*)].

The chemistry of the experimental partial melts is similar to that of kimberlites (Figs. 3 and 4). Earlier experimental work suggested that kimberlites may be formed through partial melting of H_2O-CO_2–bearing peridotite at depths greater than 3 GPa at temperatures of 1200° to 1500°C (*20*). Although CO_2 is an important factor in understanding the generation of kimberlites, our experimental results indicate that kimberlites can be formed by partial melting of H_2O-saturated peridotite at lower temperatures. Diamond-bearing kimberlites were erupted in regions underlain by continental crust older than 2.4×10^9 years (*21*), below which subcontinental mantle may be developed. Equilibration temperatures for diamond inclusions of peridotitic

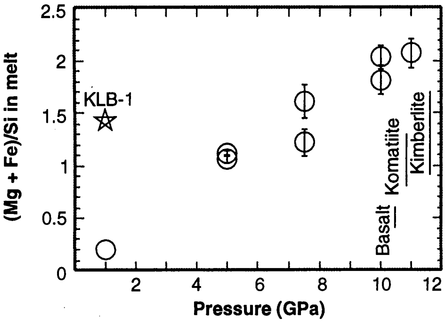

Fig. 3. (Mg + Fe)/Si molar ratios in the partial melts of H_2O-saturated KLB-1 peridotite versus pressure. The composition of subsolidus KLB-1 peridotite is represented by the star. The partial melt at 1 GPa is 60% SiO_2-bearing andesite by weight (*15*). At higher pressures, partial melts become more mafic and have (Mg + Fe)/Si molar ratios similar to those of to komatiite and kimberlites. Error bars represent ±1 SD from the mean of five or more analyses.

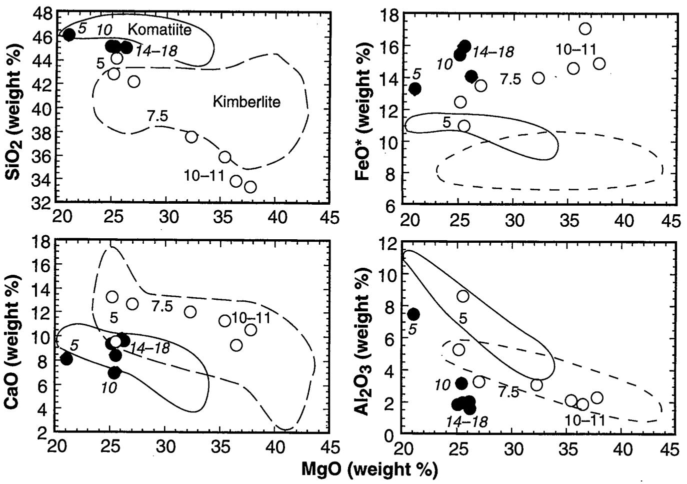

Fig. 4. MgO-variation diagrams of calculated solidus melts in the dry KLB-1 [filled circles (*17*)] and the partial melts in the wet KLB-1 (open circles, this study) with fields of estimated parental komatiite magmas (*23*) and kimberlites (*21*). Italic numerals represent experimental pressure (in gigapascals) in the dry KLB-1 system; nonitalic numerals represent pressures in the wet system. Lower FeO* abundances of the natural magmas may represent higher degrees of melting than under experimental conditions or a chemical difference of their sources.

paragenesis carried by kimberlites range from 900° to 1400°C, with most falling in the range 900° to 1100°C (*22*). The latter range is similar to our H_2O-saturated solidus temperature. Therefore, we suggest that kimberlites may have been produced by H_2O-rich fluid supplied to relatively cold subcontinental mantle at depths of 150 to 300 km.

REFERENCES AND NOTES

1. I. Kushiro, Y. Syono, S.-I. Akimoto, *J. Geophys. Res.* **73**, 6023 (1968).
2. I. Kushiro, *J. Petrol.* **13**, 311 (1972); D. H. Green, *Earth Planet. Sci. Lett.* **19**, 37 (1973).
3. T. Inoue and H. Sawamoto, in *High Pressure Research: Applications to Earth and Planetary Sciences*, Y. Syono and M. H. Manghnani, Eds. (Terra and American Geophysical Union, Tokyo and Washington, DC, 1993), pp. 323–331.
4. T. Gasparik, *J. Geophys. Res.* **98**, 4287 (1993).
5. T. Inoue, H. Yurimoto, Y. Kudoh, *Geophys. Res. Lett.* **22**, 117 (1995).
6. T. Kawamoto, R. L. Hervig, J. R. Holloway, *Earth Planet. Sci. Lett.* **142**, 587 (1996).
7. A. E. Ringwood, *Origin of the Earth and Moon* (Springer-Verlag, New York, 1979); E. Takahashi, *J. Geophys. Res.* **91**, 9367 (1986).
8. K. Hirose and T. Kawamoto, *Earth Planet. Sci. Lett.* **133**, 463 (1995); T. Kawamoto, *ibid.* **144**, 577 (1996).
9. K. J. Domanik and J. R. Holloway, *Geochim. Cosmochim. Acta* **60**, 4133 (1996).
10. J. Zhang and C. Herzberg, *J. Geophys. Res.* **99**, 17729 (1994).
11. Phase E is a nonstoichiometric hydrous crystal and was first produced in the Mg_2SiO_4-H_2O system [M. Kanzaki, *Phys. Earth Planet. Inter.* **66**, 307 (1991)]. In the wet KLB-1 peridotite system, phase E has variable Al_2O_3 abundances, from 1.5% (by weight) Al_2O_3 ($Mg_{1.4}Fe_{0.2}Al_{0.3}Si_{1.0}O_xH_y$) to 9% (by weight) Al_2O_3 ($Mg_{1.65}Fe_{0.23}Al_{0.05}Si_{1.0}O_xH_y$) [T. Kawamoto, K. Leinenweber, R. L. Hervig, J. R. Holloway, in *Volatiles in the Earth and Solar System*, K. Farley, Ed. (American Institute of Physics, Woodbury, NY, 1995), pp. 229–239.]
12. For the phase boundary between olivine and the β phase of olivine (wadsleyite), we used the result reported for nominally dry conditions by T. Katsura and E. Ito [*J. Geophys. Res.* **94**, 15663 (1989)]. The phase boundary should be changed under wet conditions. B. J. Wood [*Science* **268**, 74 (1995)] calculated such a shift in the phase boundary under wet conditions as a 0.8-GPa expansion of 500 ppm H_2O-bearing wadsleyite against olivine, based on available thermodynamic data.
13. R. G. Pacalo and J. B. Parise, *Am. Mineral.* **77**, 681 (1992); E. Ohtani, T. Shibata, T. Kubo, T. Kato, *Geophys. Res. Lett.* **22**, 2553 (1995).
14. Y. Tatsumi, *J. Geophys. Res.* **94**, 4697 (1989); K. Bose and J. Ganguly, *Earth Planet. Sci. Lett.* **136**, 109 (1995).
15. K. Hirose and T. Kawamoto, *Eos* **76**, F696 (1995).
16. T. Inoue, *Phys. Earth Planet. Inter.* **85**, 237 (1994).
17. C. Herzberg and J. Zhang, *J. Geophys. Res.* **101**, 8271 (1996).
18. K_D = (FeO/MgO) of olivine/(FeO/MgO) of melt; all Fe in the melt is assumed to be Fe^{2+} [L. L. Gee and R. O. Sack, *J. Petrol.* **29**, 1233 (1988); C. B. Agee and D. Walker, *J. Geophys. Res.* **93**, 3437 (1988)].
19. W. F. McDonough and L. V. Danyushevsky, *Eos* **76**, 266 (1995); V. S. Kamenetsky, A. V. Sobolev, J.-L. Joron, M. P. Semet, *J. Petrol.* **36**, 637 (1995).
20. D. H. Eggler, *Am. J. Sci.* **278**, 305 (1978); P. J. Wyllie, *J. Geophys. Res.* **85**, 6902 (1980); D. H. Eggler, in *Kimberlites and Related Rocks*, vol. 1, *Their Composition, Occurrence, Origin, and Emplacement*, J. Ross *et al.*, Eds. (Geological Society of Australia Special Publication 14, Carleton, Victoria, Australia, 1989), pp. 489–504.
21. R. H. Mitchell, *Kimberlites, Orangeites*, and *Related Rocks* (Plenum, New York, 1995).
22. F. R. Boyd, J. J. Gurey, S. H. Richardson, *Nature* **315**, 387 (1985).
23. E. G. Nisbet, M. J. Cheadle, N. T. Arndt, M. J. Bickle, *Lithos* **30**, 291 (1993).
24. We thank C. Herzberg for constructive discussions and a careful review. Supported by NSF grant EAR 95-06494 (J.R.H.) and the Japanese Society for the Promotion of Science (T.K.). High-pressure experiments were supported in part by NSF grant DMR 9121570. The electron probe was obtained with NSF grant 8408163.

29 October 1996; accepted 21 February 1997

Death and Transfiguration of a Triple Junction in the South Atlantic

M. Ligi, E. Bonatti,* G. Bortoluzzi, G. Carrara, P. Fabretti,
D. Penitenti, D. Gilod, A. A. Peyve, S. Skolotnev, N. Turko

Three major lithospheric plates—Antarctic, South American, and African—meet in the South Atlantic near Bouvet Island where the Mid-Atlantic Ridge (MAR), the Southwest Indian Ridge (SWIR), and the American Antarctic Ridge converge toward a fast evolving triple junction. A major magmatic pulse has recently built a new, swollen segment of the SWIR (Spiess Ridge) that is propagating toward the MAR at a rate of 4 to 5 centimeters per year, disrupting a former ridge-ridge-ridge (RRR) triple junction. A new triple junction will be established about 70 kilometers to the north when the propagating SWIR/Spiess segment will impact with the MAR, probably within the next 1 million years. The American Antarctic Ridge will take advantage of the MAR/SWIR duel by capturing an approximately 70-kilometer stretch of MAR, whereas the Antarctic plate will increase its size.

The few areas on Earth where three major lithospheric plates meet are characterized by complex, poorly understood interactions of the plate boundaries. The MAR, SWIR, and American Antarctic Ridge (AAR) converge in a triple junction (TJ) located in the Bouvet region (Fig. 1) of the South Atlantic (*1–4*). The Bouvet TJ has been interpreted as having a ridge-transform-transform (RFF) configuration (*5*) that has prevailed during most of the last 20 million years (My) (*3, 4*). Spreading half-rates estimated for the last few million years are 1.6 cm/year for MAR, 0.8 cm/year for SWIR, and 0.9 cm/year for AAR (*3*). The Bouvet TJ region is affected by one or more mantle plumes or hot spots. Bouvet Island marks the position of a plume (*6*) that may have influenced the structure and composition of the westernmost SWIR and easternmost AAR (*7*). The southernmost MAR may have been affected by the hypothetical Shona and Discovery plumes (*7–9*). We discuss the fast evolving geometry of the TJ and the extent to which mantle melting anomalies may affect this evolution.

High-resolution morphobathymetric and magnetometric coverage of the entire TJ region (Fig. 2) shows that the three accretionary plate boundaries converging toward the TJ are affected by ridge jumping, ridge overlapping, and ridge propagation (*10*), processes characteristic of fast spreading ridges but rare in slow spreading ridges. We obtained images of overlapping ridge segments (*11*) in the southernmost MAR, whereas ridge propagation is particularly clear in the westernmost SWIR (Spiess Ridge) segment (Fig. 2). This unstable geometry of the plate boundaries probably derives from the complex and variable distribution of stresses in the region arising from the interaction of three major plates. Another factor, valid at least for the MAR and SWIR, is that the rate of magma supply from the mantle is high relative to the spreading rate. Strong magmatic pulses may have triggered ridge propagation and jumping as well as the formation of an abnormally thick crust.

A thicker than normal crust is suggested by the abnormally shallow (by more than 1 km) axial topography of the SWIR segment adjacent to Bouvet Island and of the westernmost SWIR/Spiess Ridge segment. The Na-poor, H_2O- and light rare earth element–enriched composition of mid-ocean ridge basalt is consistent with the notion that hot spots influence both these SWIR segments (*7–9, 12*). Stretches of MAR between the Agulhas fracture zone at 48°S and 53°S are abnormally shallow and contain enriched mid-ocean ridge basalt with high $^3He/^4He$ ratio. These anomalies were attributed to the influence of the Discovery and Shona hot spots (*7, 8*). The MAR south of 53°S is also marked by an anomalously shallow topography. These depth anomalies, and the inferred abnormally thick

---

M. Ligi, G. Bortoluzzi, G. Carrara, P. Fabretti, D. Penitenti, Istituto Geologia Marina, CNR, via P. Gobetti 101, Bologna, Italy.
E. Bonatti, Istituto Geologia Marina, CNR, via P. Gobetti 101, Bologna, Italy, and Lamont Doherty Earth Observatory of Columbia University, Palisades, NY 10964–8000, USA.
D. Gilod, Moscow State University, Moscow, Russia.
A. A. Peyve, S. Skolotnev, N. Turko, Geology Institute, Russian Academy of Sciences, Moscow, Russia.

*To whom correspondence should be addressed. E-mail: marcol@boigm2.igm.bo.cnr.it